Simultaneous Bilateral Optical Tomography of Vascular Dynamics of the Breast Using High-Density Sensing Arrays

Christoph H. Schmitz[1], Rehman Ansari[2], Rabah Al Abdi[2], Randall Andronica[2], Yong Xu[2,3], Harry L. Graber[2,3], Yaling Pei[3], Mark Farber[2], Kuppuswamy Jagarlamudi[2], and Randall L. Barbour[2,3]

[1]NIRx Medizintechnik GmbH, Germany; [2]SUNY Downstate Medical Ctr., USA; [3]NIRx Medical Technologies LLC, USA

ABSTRACT

An optical tomography system was developed that allows the simultaneous bilateral imaging of the breasts' vascular dynamics with a high spatial probing density (2096 measuring channels per wavelength per breast). The system features novel arrays of fiber-optic probes, which afford high-fidelity optical contact in a well-defined geometry, and which conform to a wide range of breast shapes and sizes without undue compression or the use of coupling fluids. The sensing arrays use strain gauges to monitor the compression of the breasts and to measure the tissue's reaction to pressure-modulating patient maneuvers.

The system is described, and preliminary experimental results from combined optical/strain measurements on the healthy breast are shown.

OCIS codes: 170.3890 (Medical optics instrumentation), 170.6960 (Tomography)

MOTIVATION

Our strategy for increasing diagnostic power of optical breast imaging:

- Imaging of hemodynamic activity of breast vasculature during rest or in response to provocation allows identification of tissues with deranged autoregulation (e.g., cancerous and pre-cancerous states), with high contrast [1]
- Simultaneous dual-breast imaging allows for paired comparison between diseased and healthy tissue, thus increasing statistical robustness [2]
- Multitude of hemodynamic metrics may be considered for use as uni- and multivariate disease predictors [3]

Previously described instrumentation was used for method evaluation, and demonstrated:

- Instrumental feasibility of dual-breast imaging
- Potentially high diagnostic power for many uni-variate and multivariate diagnostic metrics based on bilateral dynamic contrasts

Some practical shortcomings also became clear, which were addressed in the new imager design:

- Patients were required to lie prone, which for many was uncomfortable, and which interfered with the proper performance of provocation protocols, such as the quantitative Valsalva maneuver.
- fixed-size plastic cups as fiber-optic interface:
  - ⇒ limited anatomical adaptability: good optical contact could be achieved only for a subset of breast sizes and shapes;
  - ⇒ circular cross-section maximizes measuring distances in the coronal plane, thus decreasing the achievable signal-to-noise ratio.
- Fairly sparse optode arrangement of 31 sources (S) x 31 detectors (D) per breast. Rigid dual-cup probe holder accommodated only limited breast sizes, or only a portion of the breast

To alleviate these shortcomings, the new instrument was designed with the following features:

- Cart-based design and probe holders on two articulated arms, for independent positioning of the fibers on each breast, to allow imaging the subject in a comfortable sitting position.
- Increased no. of channels: 32S x 64D per breast (total of 2 x 2048 Ch. x 2 Wavelengths @ 1.8Hz)
- Measuring head design: clamshell mechanism
  - allows mild compression for better transmission
  - accommodates large range of breast sizes
  - allows pressure modulation
  - high spatial sensing density
- Integrated strain gauges measure pressure/displacement of tissue

INSTRUMENTATION

The instrument design (see Fig. 1) expands on proven technology described before [4]:

- **Detection**: 2x 64-channel detector modules with Si photodiodes, adaptive gain switching, and analog lock-in amplification for demodulation of two frequency-encoded wavelengths. Signal sampling by 4 64-analog-channel data acquisition boards (National Instruments PCI 6033).
- **Illumination**: 2x fiber pigtailed laser diodes (400 mW_{max}, 760 nm, 830 nm, from High Power Devices, Inc., NJ), combined by dichroic mirrors (OZ Optics, Canada) and focused into a home-built optical switch (OS) [2,4]. OS uses rotating 2-mirror stack for parallel multiplexed illumination of both breasts through two source-fiber arrays. Physical separation of breasts sufficiently suppresses potential optical crosstalk between measuring sites.
- **Probe holders**: A Clamshell design comprising mechanical fingers to arrange optodes in linear arrays of four (Fig. 1c) on the superior breast surface. The lower half of the device consists of 4 metal fingers, each carrying 8 fibers, forming the lower breast support. Horizontal distance between top and bottom fingers is variable, via a single adjustment screw, to accommodate different breast sizes. The upper half of the clamshell is formed by 8 cantilevered metal rods (Fig 1b,c) which can be adjusted to accommodate different breast sizes and to apply a controlled pressure to the tissue.
- **Strain gauges**: 8 semiconductor strain gauges (SS-090-060-500P by Micron Instruments, Inc., CA) are incorporated into each measuring head to monitor pressure exerted onto the breast tissue by sensing minute bending in the support rods, causing changes in resistance (Fig. 1d). Gauge resistance changes linearly with the force applied to the rod (5.7 Ω/N, linearity better than 1% over a range of 15N, see Fig. 1e). Nominal resting resistance of the devices: 540 Ω @ 25.5°C; load-free mounted resistance (offset) ~ 410 Ω. Individual gauge response differences (stable, within 10%) are calibrated. Gauges are read out with a voltage divider and sampled by a data acquisition board (USB 6218 by National Instruments Corp, TX). Achievable measurement sensitivity is 16 mN.

Fig. 1: Instrument Setup

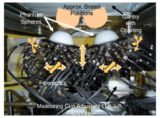

(a) Previous dual-breast interface

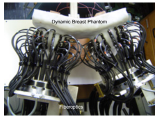

(b) New dual-breast interface w/ dynamic phantom

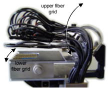

(c) Side view of new fiber holder

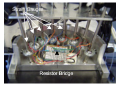

(d) Position of strain gauges

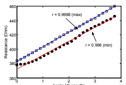

(e) P-doped semiconductor strain gauge response

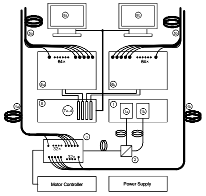

(f) Breast imager schematic diagram

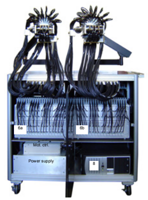

(g) Breast imager photograph.

Imager components: 1: Laser controller, 1a,b: Laser driver 760 nm and 830 nm, resp., 2: Wavelength combiner, 3: Optical switch, 4a,b: Illumination fibers for left and right breast, 5a,b: Detection fibers for left and right breast, 6 a,b: Optical detectors for left and right breast, 7a..d: Data acquisition cards, 8: Personal computer, 8a,b: Display of left, right breast data.

Fig. 2: FEM Model

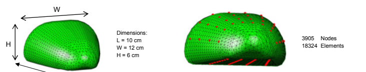

(a) FEM mesh details

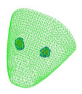

(b) Model and targets. Inclusion dimension: 1.2 cm

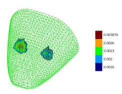

(c) Simulated result: Reconstructed absorption image

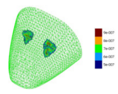

(d) Phantom result: Reconstructed Hb-Oxy GLM coefficient image

Fig. 3: New Instrument Phantom Results

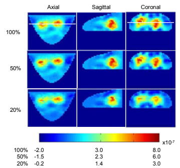

(a) Reconstructed GLM coefficient images

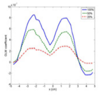

(b) Reconstructed concentration change in inclusions

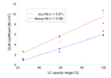

(c) Reconstructed vs. programmed concentration change

Fig. 4: New Instrument Volunteer Results

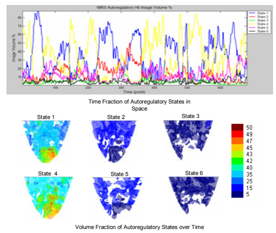

(a) Baseline activity.

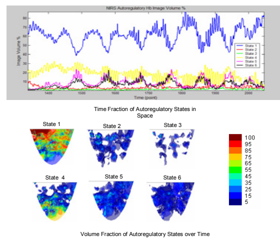

(a) Response to Carbogen (5% CO_2) .

ACKNOWLEDGMENTS

We would like to acknowledge and thank Naresh Patel and Rahul Valluru for their help on this project.
This research was supported by the National Institutes of Health (NIH) under grants 1R43CA91725-1A1, R21-HL67387, R21-DK63692, and R41-CA96102; by the U.S. Army under grant DAMD017-03-C-0018; by the New York State Department of Health; and by the Susan G. Komen Foundation under grant IMG0403022.

Fig. 5: Patient Study

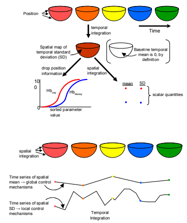

(a) Derivation of integrated baseline (autoregulation) metrics.

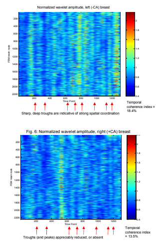

(b) Derivation of wavelet-based (temporal coherence) metrics.

Tab. 1: Mean values and significance levels of the explored functional metrics.

[illegible]	[illegible]

TSDSMts, Temporal standard deviation of spatial mean time series (amplitude of regional blood redistribution [illegible]); TSDSSDts, temporal standard deviation of spatial standard deviation time series (amplitude of autoregulation); SMTSDi, spatial mean of temporal standard deviation image (amplitude of mixed control); [illegible] deviation image (heterogeneity of mixed control). Statistically significant results (p < 0.05) are marked by color.

Tab. 2: Multivariate metrics explored in study.

Formulation	$N_{subjects}$	$N_{metrics}$	Hb States Included	Data Groups Included	Sens. (%)	Spec. (%)	PPV (%)	NPV (%)	
(1) Diff./Max.	21	3	Oxy (2), Total (1)	1, 3	100	90.9	90.1	100	All Subjects
					87.5	90.0	87.5	90.0	LOOCV[a]
(2) Diff.*Max	21	3	Oxy (1), Deoxy (1), Total (1)	1, 2, 3	100	81.8	83.3	100	All Subjects
					70.0	90.0	87.5	75.0	LOOCV
(3) Diff.*Max.	37	5	Oxy (3), Deoxy (1), Total (1)	1, 2	100	87.0	82.4	100	All Subjects
					85.7	73.9	66.7	89.5	LOOCV
(4) Diff./Max.	37	3	Oxy (1), Deoxy (2)	2	50.0	87.0	74.1	70.0	All Subjects

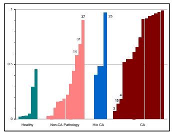

(c) Results of prospective study using predictor no. 4 in Tab. 2.

Tab. 3: Diagnostic accuracy parameters for all metrics.

Form.	$N_{metrics}$	Grps.	Sens. (%)	Spec. (%)	PPV (%)	NPV (%)
diff/max	3	1, 3	69.2	78.9	69.2	78.9
diff*max	3	1, 2, 3	52.9	68.4	60	61.9
diff*max	5	1, 2	61.5	76.2	61.5	76.2
diff/max	3(w)	3	81.3	86.4	81.3	86.4

Tab. 5: Lesion details for FP and FN patients.

ID	Lesion details
14	[illegible]
31	[illegible]
37	[illegible]
25	[illegible]
3	[illegible] T1, N1, MO? (2 nodules in lung follow up on nodules)- STAGE II. LOCATION: grouped calcification in left breast @ 11o'clock. TYPE:Invasive Ductal CA (Grade III) with Lymphatic Permeation by Tumor, DCIS with cribriform calcification. ER 3+ , PGR 3+, P-53 3+, KI-67 3+, Her2/neu NEG.
15	Left Breast Ca. s/p lumpectomy (2003), s/p chemotherapy (nov-2004), not responding to chemo and awaiting surgery. HTN [hypertension], asthma (mild intermittent). T3, N1, MO - stage IIIA. Location: 6cm, irregular, high-density mass withh an indistinct margin in the left breast at 11 o'clock in the anterior depth, 1.3 cm round high density mass with a circumscribed margin in the left breast at 9 o'clock in the posterior depth. Focal asymmetric density in the left breast at 11 o'clock in the posterior depth. Type: mucinous (colloid) adenocarcinoma (7x4x3), minor part of tumor highly cellular and mucin dissecting the stroma. LN 3/12 + - T3, N1, MX
4	Left Breast Carcinoma (12 o'clock) with left axillary lymph nodes metastasis, s/p neo-adjuvant chemotherapy (adriamycin and cytoxan) around 7/05. HTN, DM, Glaucoma, arthritis. T2, N1, Mx - STAGE II. Location: left breast, 12 o'clock position, 6cm from the nipple. TYPE: invasive ductal carcinoma, Grade II. er+, PR +, Her2 +, Ki-67 +, with LN positive.

Tab. 4: Study group demographics.

Training Set	Age (years)					BMI				
	N	Mean	SD	Range	p^{a}	N	Mean	SD	Range	p^{a}
CA	14	47.9	12.7	29-70	0.39	14	28.7	5.5	29-70	0.50
Non-CA	23	44.7	8.7	26-62		19[b]	30.1	6.3	31-62	

Confirmation/ Test Set	Age (years)					BMI				
	N	Mean	SD	Range	p^{a}	N	Mean	SD	Range	p^{a}
CA	16	52.9	11.6	37-71	0.11	15	29.3	4.6	23-36	0.96
Non-CA	20	47.1	9.3	32-69		16	29.2	7.2	21-49	

Tab. 6: Menopausal status.

pre:post	non-CA	CA
training	12:6	11:3
test	12:9	8:8

METHODS

- Subject demographics for the measurements are summarized in Tab. 4
- The dynamic phantom consisted of a malleable silicone rubber, with optical properties matching those of breast tissue, into which electrochromic cells were embedded. Electronic control of the inclusions allows precise mimicking of local changes in Hb_{oxy} and Hb_{red} [5].
- 3D Images were reconstructed with a first-order solution of the diffusion equation [6]
- Concentration changes in the reconstructed phantom data were determined with a General Linear Model (GLM)
- Healthy-volunteer measurements using the new setup were analyzed according to a recently described algorithm to extract autoregulatory states of tissue (also see Posters BMD1, BSuE61, BSuE57)
- The prospective patient study performed with the first-generation dual-breast imager was analyzed using a variety of uni- and multivariate disease predicting metrics derived earlier on a training set of patients. The metrics are based on relative left-vs.-right differences for (1) spatiotemporally averaged baseline activity, (2) the spatial synchrony of low-frequency rhythms during baseline, (3) the pressure-induced blood volume and oxygenation shifts (see Fig. 5a,b and Tab. 1).
- For multivariate predictors, a logistic regression algorithm was used to determine the optimal weighting coefficients.

RESULTS AND DISCUSSION

Validation studies for new imager:

- A FEM mesh of the compressed breast was developed (Fig. 2). Simulations yield localization of inclusions with high accuracy for the given measurement geometry.
- Phantom measurements demonstrate (1) accurate inclusion localization and (2) highly linear relation between programmed and reconstructed inclusion optical density (Fig. 3).
- Healthy volunteer studies demonstrate capability to extract autoregulatory tissue features as shown in Fig. 4.
  - ⇒ *These results demonstrate the new technology's capability of high-fidelity data capture and functional feature extraction.*
  - ⇒ *Dense spatial sampling of the breast and good adaptability to various breast sizes were successfully demonstrated.*

Prospective clinical study (previous imager):

- Prospective study on 4 patient groups (healthy, non-CA pathology, history of CA, CA)
- Multivariate predictors were derived from results on a previously obtained training set of data [3] (Fig. 5)
- Whereas multi-variate disease predictors 1-3 in Tab. 2 yielded the best diagnostic power on the training set, they turned out not to be the optimal choice for the test set. Most successful here was a purely wavelet transform-based formulation (row 4 of Tab. 2). We attribute this discrepancy to (1) the age mismatch in the study subgroups from test and training set – specifically training non-CA vs. test CA (p = 0.02) – and (2) a strong mismatch in the numbers of pre- and postmenopausal participants in the CA groups (bias of pre-menopausal women in training set, Tab. 6). We expect to these difficulties in future dataset to be alleviated by larger enrollment numbers.
- Fig. 5c shows a histogram of the computed p values for the most successful metric. The threshold for disease prediction is set at 0.5. It can be seen that while healthy volunteers are all correctly identified, our false positive results occur only for participants in group 2 (other, non-CA lesion) and Group 3 (history of CA). We would like to note that, although at the time of study considered CA-free, pt. 25 was diagnosed with a relapse about a year later so that this FP result could be explained by unknown presence of cancerous tissue at the time of imaging. Tab. 5 lists the lesion details for all our FP and FN cases.
- Predictor no. 4 yields sensitivity and specificity of 81% and 86%, respectively, and positive and negative predictive power of 81% and 86%, respectively.
  - ⇒ *A host of functional metrics of high diagnostic accuracy are derivable from L-R comparison of breast tissue hemodynamics*
  - ⇒ *Multivariate predictors have been demonstrated to achieve high diagnostic power for disease prediction in a prospective study*
  - ⇒ *Age differences and related menopausal status is seen as having a significant impact on the predictive power of our functional metrics*

REFERENCES

[1] R.L. Barbour, H.L. Graber, Y. Pei, S. Zhong, C.H. Schmitz, "Optical tomographic imaging of dynamic features of dense-scattering media," *JOSA A* **18**, 3018-3036 (2001).
[2] C.H. Schmitz, D.P. Klemer, R.E. Hardin, M.S. Katz, Y. Pei, H.L. Graber, M.B. Levin, R.D. Levina, N.A. Franco, W.B. Solomon, R.L. Barbour, "Design and implementation of dynamic near-infrared optical tomographic imaging instrumentation for simultaneous dual-breast measurements," *Applied Optics* **44**, 2140-2153 (2005).
[3] Y. Pei, H.L. Graber, M. Farber, C.H. Schmitz, Y. Xu, P. Toubas, N. Patel, M.S. Katz, W.B. Solomon, and R.L. Barbour, "Tumor detection by simultaneous bilateral diffuse optical tomography (DOT) breast imaging," Poster No. 82 at Fifth Inter-Institute Workshop on Optical Diagnostic Imaging from Bench to Bedside at the National Institutes of Health (Bethesda, MD, September 25-27, 2006).
[4] C.H. Schmitz, M. Löcker, J.M. Lasker, A.H. Hielscher, R. L. Barbour, "Instrumentation for fast functional optical tomography," *Review of Scientific Instruments*, Vol. 73, pp. 429-439 (2002).
[5] R.L. Barbour, H.L. Graber, Y. Xu, Y. Pei, R. Ansari, M.B. Levin, and M. Farber, "Diffuse Optical Tissue Simulator (DOTS): An experimental calibrating system for functional DOT imaging," Poster No. 76 at Fifth Inter-Institute Workshop on Optical Diagnostic Imaging from Bench to Bedside at the National Institutes of Health (Bethesda, MD, September 25-27, 2006).
[6] Y. Pei, H.L. Graber, R.L. Barbour, "Influence of systematic errors in reference states on image quality and on stability of derived information for DC optical imaging," *Applied Optics*, Vol. 40, pp. 5755-5769 (2001).